recent epidemiological studies reveal no correlation of hearing loss and osteoporosis in elderly women [18], a finding that seems counterintuitive given that hearing largely depends on bone.

*Opg*$^{-/-}$ mice develop osteopenia due to enhanced differentiation of osteoclasts [19–22]. To gain deeper insight into the role of bone remodeling in hearing, we asked if auditory ossicles are susceptible to osteoclastic bone resorption in *Opg*$^{-/-}$ mice and whether auditory function is impaired.

## Materials and methods

### *Mice*

Female *Opg*$^{-/-}$ and heterozygous control mice on a C57BL6 background were purchased from Clea Japan. All experiments were conducted in accordance with institutional review board-approved protocols.

### *Morphological analyses*

Mouse skulls were fixed in 4% paraformaldehyde. For macroscopic analysis, auditory ossicles were isolated by removing the temporal bone, stained for tartrate-resistant acid phosphatase (TRAP) activity using the Leukocyte Acid Phosphatase Kit (Sigma), and observed using a SMZ1500, stereoscopic zoom microscope configured with the Eclipse 90i digital camera system (Nikon). For histological analysis, skulls were decalcified in 0.5 M EDTA for 1 week, and the temporal bones containing auditory ossicles were trimmed and embedded in paraffin. Frontal sections of 5 μm thickness were stained with hematoxylin–eosin (HE) and for TRAP activity.

### *Radiographical analyses*

Each isolated malleus was embedded in melted 8% gelatin in a segment of a plastic drinking straw. After solidifying the gelatin at 4°C, mallei were scanned using micro-computed tomography (μCT) instrumentation (μCT-40, Scanco Medical AG, Switzerland). Based on two-dimensional data from scanned slices, cortical thickness was calculated by setting the volume of interest (VOI) to the entire malleus. Tibial cortical BMD was measured using a CT scanner (*LaTheta* LCT-100, Aloka, Japan) with isolated bilateral tibiae.

### *Auditory brain-stem response (ABR) measurement*

A needle electrode was subdermally inserted at the vertex along the dorsal midline of the scalp between the external auditory canals. The reference electrode was placed below the pinna of the left ear, and the ground electrode was inserted below the contralateral ear. The sound stimulus consisted of a 1 ms tone burst with a rise–fall time of 0.1 ms. For each stimulus, ABR waveforms were recorded for 12.8 ms at a sampling rate of 40,000 Hz using 50–5000 Hz bandpass filter settings, and waveforms from 256 stimuli at a frequency of 9 Hz were averaged. ABR waveforms were recorded in 5-dB sound pressure level (SPL) intervals down from a maximum amplitude until no waveform could be observed using Scope software of the PowerLab system (PowerLab2/20, AD Instruments, Australia). ABRs were performed on mice aged 6, 10, and 15 weeks at the following frequencies: 2, 4, 12, and 20 kHz. ABRs were measured under anesthesia induced by intraperitoneal injection of 0.01 ml/g body weight of 2.5% avertin. The researcher who measured ABRs was unaware of the identities of the animals.

### *Statistical analysis*

Statistical comparisons were performed using Student's *t* test and analysis of variance, where appropriate.

## Results

To examine the morphology of the auditory ossicles in *Opg*$^{-/-}$ mice, we isolated mallei, incudes, and stapes from the middle ear cavities of 10-week-old *Opg*$^{-/-}$ mice and from wild-type and heterozygous controls. We observed that the junction between the stapes and the oval window of the cochlea was tighter in *Opg*$^{-/-}$ mice compared to control mice. Ossicles from *Opg*$^{-/-}$ and control mice were stained for TRAP activity, which is a marker for osteoclasts and resorption lacunae. Compared to wild-type and heterozygous controls, all three ossicles in *Opg*$^{-/-}$ mice were more heavily stained for TRAP activity and exhibited thinning, particularly at the malleal manubrium, malleal processus brevis, incus body, and stapedial arch (Fig. 1a). Furthermore, the stapedial footplate was thinner and broader at the periphery in *Opg*$^{-/-}$ mice (Fig. 1a, Stapes, top view). Such thinner parts of ossicles, especially of the stapes, exhibited intense TRAP staining (Fig. 1a).

To further analyze osteoclasts in the auditory ossicles, histological sections of the temporal bone from wild-type, heterozygous, and *Opg*$^{-/-}$ mice were stained for TRAP activity. Compared to wild-type and heterozygous controls, TRAP-staining was much stronger in both auditory ossicles and the otic capsule in *Opg*$^{-/-}$ mice (Fig. 1b and data not shown). We next quantitated the number of TRAP-positive multinucleated cells (MNCs) in wild-type, heterozygous, and *Opg*$^{-/-}$ mice (Fig. 1c). The number of TRAP-positive MNCs was significantly higher in *Opg*$^{-/-}$ mice than in controls, suggesting that osteoclastic bone resorption of auditory ossicles is dramatically enhanced in *Opg*$^{-/-}$ mice.

We also histologically examined the junction between the stapes and the otic capsule in heterozygous and *Opg*$^{-/-}$ mice. The ligament between the stapedial footplate and otic capsule was intact in heterozygous mice (Fig. 2a), while no ligament was seen in *Opg*$^{-/-}$ mice, and the junction was replaced with bone tissue fusing the stapes and otic capsule (Fig. 2b).

We next examined the auditory ossicles radiographically. Imaging using μCT of isolated mallei confirmed massive erosion in ossicles of *Opg*$^{-/-}$ mice, which was not observed in heterozygous mice (Fig. 3a). Based on the μCT images, cortical thickness of mallei was calculated in *Opg*$^{-/-}$ mice and controls. Malleal cortical thickness observed in *Opg*$^{-/-}$ mice was significantly lower than that seen in heterozygous controls (Fig. 3b). As expected, tibial cortical BMD of *Opg*$^{-/-}$ mice was also lower than that seen in heterozygous mice (Fig. 3c). Consistent with the histological data, these

Fig. 1. Excess bone remodeling of auditory ossicles. (a) Biomicroscopic photographs showing auditory ossicles from 10-week-old wild-type (+/+), heterozygous (+/−), and *Opg*$^{-/-}$ (−/−) mice ($n = 6$ or more for each genotype). Ossicles were stained for TRAP activity (red). Arrowheads indicate the malleal manubrium, incus body, and stapedial footplate. Scale bar, 100 μm. (b) Histological sections of auditory ossicles in the middle ear cavity from 15-week-old *Opg*$^{-/-}$ mice ($n = 2$ per genotype). HE and TRAP activity staining is shown. TRAP-positive areas in the malleus (M), incus (I), and stapes (S) are indicated by arrowheads, and those in the otic capsule by arrows. tm, tympanic membrane. Scale bar, 100 μm. (c) The number of TRAP-positive MNCs in mallei from wild-type, heterozygous, and *Opg*$^{-/-}$ mice ($n = 5$ for +/+, $n = 4$ for +/− and −/−). $^{\#}P < 0.001$.

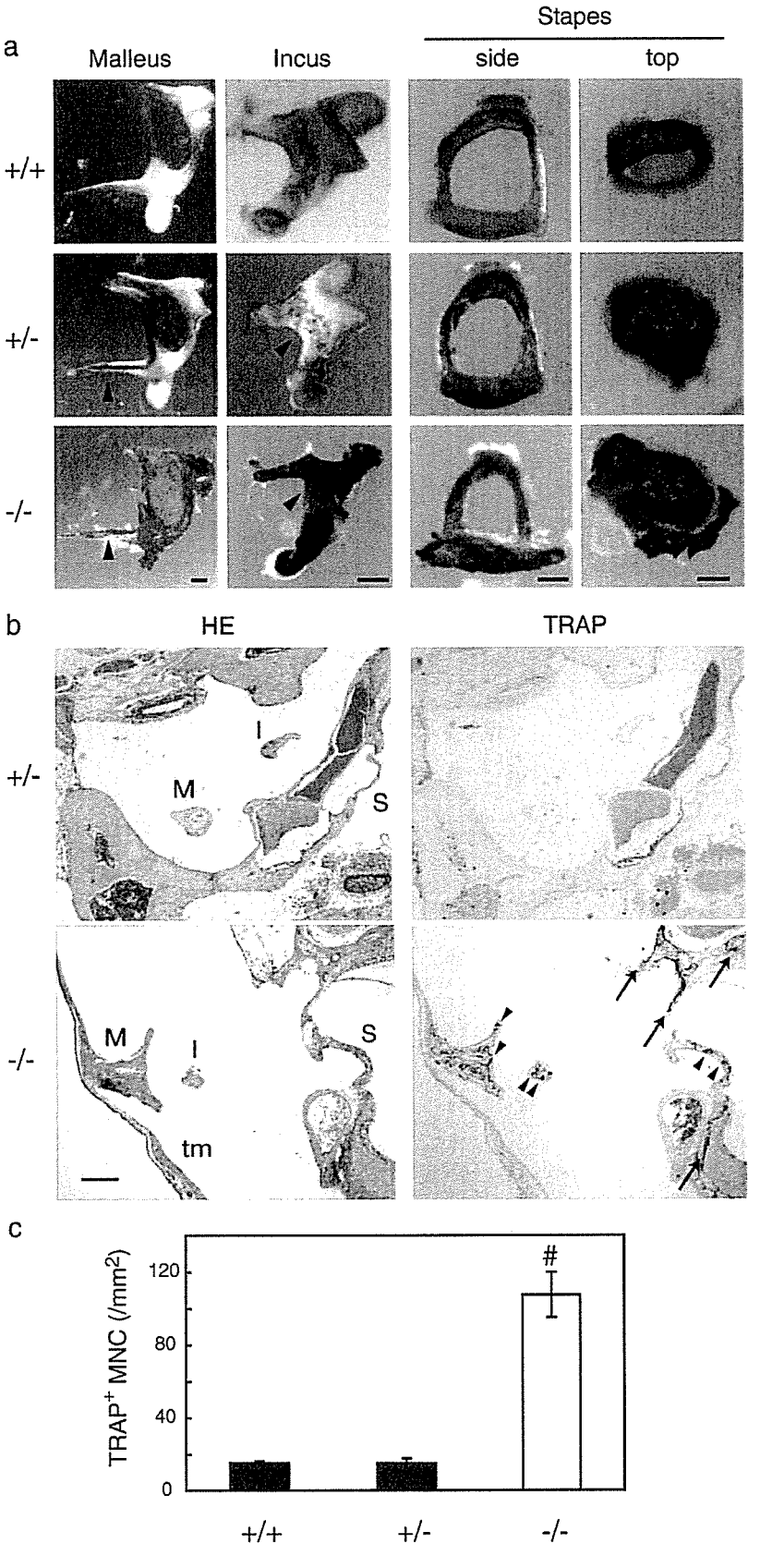
a
Malleus
Incus
Stapes
side
top
+/+
+/-
-/-
b
HE
TRAP
+/-
M
I
S
-/-
M
I
S
tm
c
TRAP+ MNC (/mm2)
120
80
40
0
#
+/+
+/-
-/-

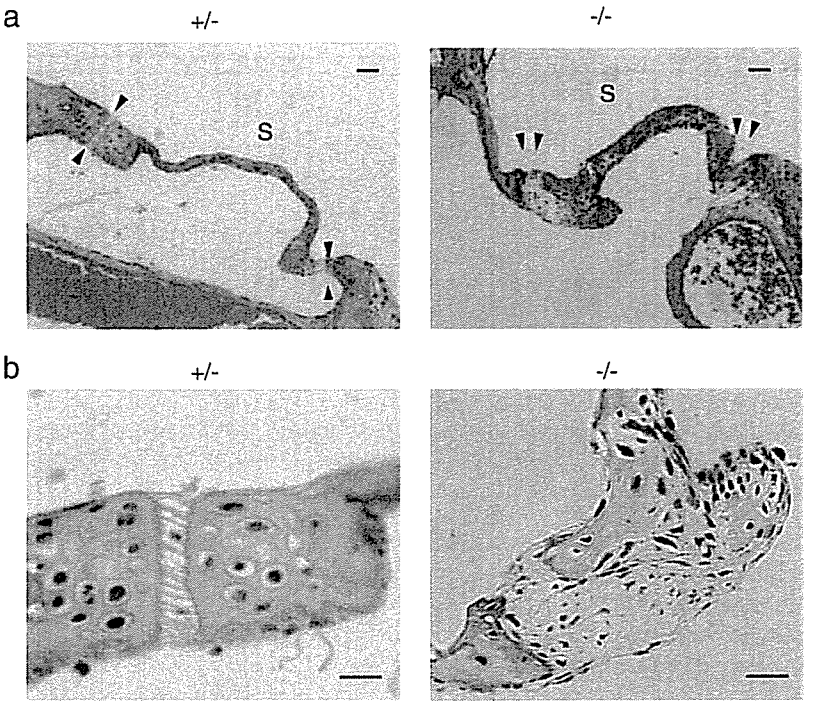


Fig. 2. Histological sections of the stapedial–cochlear junction (arrowheads). Staining is HE ($n$ = 3 for each genotype). Scale bar, 25 μm.

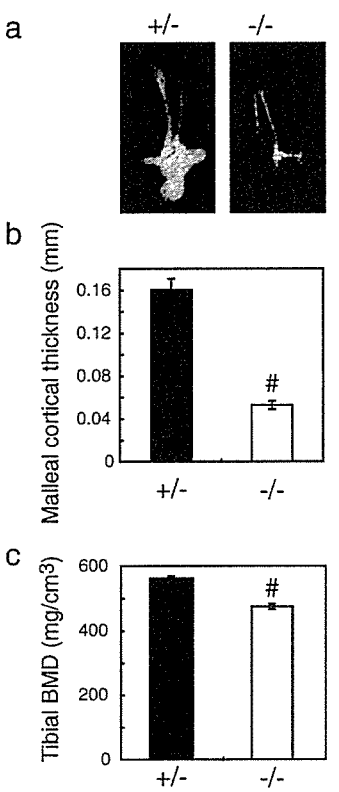


Fig. 3. Radiographical analysis of auditory ossicles and tibia. (a) Representative μCT images of the malleus from 8-week-old mice ($n$ = 5 for +/− and $n$ = 5 for −/−). (b) Malleal cortical thickness of mice described in panel a. (c) Tibial cortical BMD of mice described in panel a. $^{\#}P < 0.001$, versus heterozygous mice.

data suggest that osteoclastic bone resorption of auditory ossicles is elevated in the absence of OPG, leading to bone loss.

To test whether bone loss observed in $Opg^{-/-}$ mice is associated with differences in hearing ability, we assessed ABR thresholds at 6, 10, and 15 weeks of age in heterozygous and $Opg^{-/-}$ mice. ABR threshold was determined as the minimum sound pressure level (SPL) giving reproducible waveforms. At 6 weeks of age, the average ABR threshold of $Opg^{-/-}$ mice was similar to that of heterozygous littermate controls at frequencies from 2 to 20 kHz. However, at 10 weeks of age, $Opg^{-/-}$ mice began showing higher (i.e., worse) thresholds than controls (Fig. 4). By 15 weeks, the differences were even greater, with $Opg^{-/-}$ mice being more than 20 decibels (dB) less sensitive than heterozygous controls at the highest frequency of 20 kHz (Fig. 4). These data suggest that excessive bone remodeling can result in progressive hearing loss.

## Discussion

In adult $Opg^{-/-}$ mice, we observed erosion of the malleus, incus, and stapes. Furthermore, TRAP activity was detected in all the three ossicles and the otic capsule of $Opg^{-/-}$ mice, indicating that osteoclastic bone resorption of auditory ossicles is elevated. It is unclear whether certain specific areas within each ossicle are preferentially resorbed or not. We also observed that $Opg^{-/-}$ mice show progressive hearing loss. The precise mechanisms of hearing loss in these mice are currently unknown. Since hearing loss in each animal was progressive, sudden loss of articulation between auditory ossicles is not likely to be the cause of impairment. We observed extensive resorption

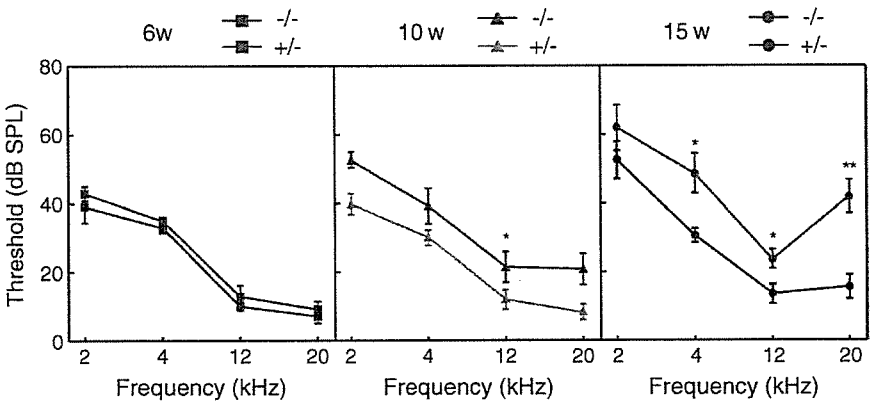


Fig. 4. Progressive increase in ABR thresholds of $Opg^{-/-}$ mice. Data points for thresholds at 2, 4, 12, and 20 kHz in $Opg^{-/-}$ mice and heterozygous controls at the ages of 6 ($n = 5$ each), 10 ($n = 7$ each), and 15 ($n = 7$ each) weeks. Significant differences between 15-week-old $Opg^{-/-}$ and heterozygous control mice are indicated with asterisks ($*P < 0.05$, $**P < 0.01$).

of the malleal processus brevis in $Opg^{-/-}$ mice, but the malleal processus brevis is dispensable for hearing function [2]. In $Opg^{-/-}$ mice, we observed that stapedial fixation, namely, the ligaments between the stapes and the otic capsule, was replaced with bone tissue. Among the observed morphological alterations including thinning of the malleal manubrium and incus body, stapedial fixation is the most likely cause of hearing loss in $Opg^{-/-}$ mice. Clinically, hearing loss in otosclerosis can be cured by surgical intervention at the stapedial–cochlear junction, indicating the importance of this junction in hearing.

OPG deficiency has been found in patients with juvenile Paget's disease, which is also known as idiopathic hyperphosphatasia [23–27] and characterized by markedly increased bone turnover. Paget disease of bone is a distinct and much more common disease than juvenile Paget's disease, characterized by excessive osteoclastic bone resorption followed by compensatory increase in osteoblastic bone formation [28]. Curiously, hearing is affected in approximately 50% of cases of Paget disease of bone involving the skull [29]. Hearing loss in patients with otosclerosis and Paget disease of bone could be due to the increased bone formation, which narrows the internal auditory canal and causes nerve atrophy. On the other hand, hearing loss has been positively correlated with loss of bone density in the otic capsule [30, 31]. Similarly, activating mutations in *TNFRSF11A*, which encodes RANK, cause expansile skeletal hyperphosphatasia, which features deafness in infancy or early childhood [32]. Familial expansile osteolysis, which is also caused by mutation in *TNFRSF11A* [33], is also associated with deafness.

Recent reports show that OPG is highly expressed in cochlear soft tissues and secreted into the perilymph and surrounding bone [34]. Furthermore, OPG levels increase with age in women [35–37]. The apparent lack of association between osteoporosis and hearing loss in humans [18] implies that the auditory ossicles and the otic capsule may be protected from osteoclastic bone resorption by OPG even in patients with postmenopausal and age-related osteoporosis. In conclusion, these data reveal a critical role for OPG as an "audioprotegerin" in maintaining quality of bone conduction by protecting auditory ossicles and the otic capsule from bone resorption. Impaired production of OPG in the temporal bone may be a risk factor for hearing loss.

## Acknowledgments

We thank Shumpei Niida, Kyoji Ikeda, and Minako Sato for helpful discussions and Neelanjan Ray and Elise Lamar for critical reading of the manuscript. This work is supported by Grant-in-Aid for Young Scientists B (17791198 to SK) and Grant-in-Aid for Scientific Research B (17390420 to KM) from JSPS, and a Keio University Special Grant-in-Aid for Innovative Collaborative Research Projects.

## References

[1] Mallo M. Formation of the middle ear: recent progress on the developmental and molecular mechanisms. Dev Biol 2001;231:410–9.
[2] Zhang Z, Zhang X, Avniel WA, Song Y, Jones SM, Jones TA, et al. Malleal processus brevis is dispensable for normal hearing in mice. Dev Dyn 2003;227:69–77.
[3] Teitelbaum SL, Ross FP. Genetic regulation of osteoclast development and function. Nat Rev Genet 2003;4:638–49.
[4] Karsenty G, Wagner EF. Reaching a genetic and molecular understanding of skeletal development. Dev Cell 2002;2:389–406.
[5] Franzoso G, Carlson L, Xing L, Poljak L, Shores EW, Brown KD, et al. Requirement for NF-κB in osteoclast and B-cell development. Genes Dev 1997;11:3482–96.
[6] Grigoriadis AE, Wang ZQ, Cecchini MG, Hofstetter W, Felix R, Fleisch HA, et al. c-Fos: a key regulator of osteoclast-macrophage lineage determination and bone remodeling. Science 1994;266:443–8.
[7] Matsuo K, Owens JM, Tonko M, Elliott C, Chambers TJ, Wagner EF. *Fosl1* is a transcriptional target of c-Fos during osteoclast differentiation. Nat Genet 2000;24:184–7.
[8] Takayanagi H, Kim S, Koga T, Nishina H, Isshiki M, Yoshida H, et al. Induction and activation of the transcription factor NFATc1 (NFAT2) integrate RANKL signaling in terminal differentiation of osteoclasts. Dev Cell 2002;3:889–901.
[9] Matsuo K, Galson DL, Zhao C, Peng L, Laplace C, Wang KZ, et al. Nuclear factor of activated T-cells (NFAT) rescues osteoclastogenesis in precursors lacking c-Fos. J Biol Chem 2004;279:26475–80.
[10] Simonet WS, Lacey DL, Dunstan CR, Kelley M, Chang MS, Luthy R, et al. Oteoprotegerin: a novel secreted protein involved in the regulation of bone density. Cell 1997;89:309–19.

[11] Yasuda H, Shima N, Nakagawa N, Yamaguchi K, Kinosaki M, Mochizuki S, et al. Osteoclast differentiation factor is a ligand for osteoprotegerin/osteoclastogenesis-inhibitory factor and is identical to TRANCE/RANKL. Proc Natl Acad Sci U S A 1998;95:3597–602.
[12] Martin TJ, Sims NA. Osteoclast-derived activity in the coupling of bone formation to resorption. Trends Mol Med 2005;11:76–81.
[13] Cooper C. Epidemiology of osteoporosis. Primer on the Metabolic Bone Diseases and Disorders of Mineral Metabolism. The American Society for Bone and Mineral Research; 2003. p. 307–13.
[14] Adams PF, Benson V. Current estimates from the National Health Interview Survey, 1991. Vital Health Stat 1992;10:1–232.
[15] Henkin RI, Lifschitz MD, Larson AL. Hearing loss in patients with osteoporosis and Paget's disease of bone. Am J Med Sci 1972;263:383–92.
[16] Haboubi NY, Hudson PR. Factors associated with Colles' fracture in the elderly. Gerontology 1991;37:335–8.
[17] Clark K, Sowers MR, Wallace RB, Jannausch ML, Lemke J, Anderson CV. Age-related hearing loss and bone mass in a population of rural women aged 60 to 85 years. Ann Epidemiol 1995;5:8–14.
[18] Helzner EP, Cauley JA, Pratt SR, Wisniewski SR, Talbott EO, Zmuda JM, et al. Hearing sensitivity and bone mineral density in older adults: the Health Aging and Body Composition Study. Osteoporos Int 2005;16:1675–82.
[19] Bucay N, Sarosi I, Dunstan CR, Morony S, Tarpley J, Capparelli C, et al. *Osteoprotegerin*-deficient mice develop early onset osteoporosis and arterial calcification. Genes Dev 1998;12:1260–8.
[20] Mizuno A, Amizuka N, Irie K, Murakami A, Fujise N, Kanno T, et al. Severe osteoporosis in mice lacking osteoclastogenesis inhibitory factor/osteoprotegerin. Biochem Biophys Res Commun 1998;247:610–5.
[21] Amizuka N, Shimomura J, Li M, Seki Y, Oda K, Henderson JE, et al. Defective bone remodelling in osteoprotegerin-deficient mice. J Electron Microsc (Tokyo) 2003;52:503–13.
[22] Nakamura M, Udagawa N, Matsuura S, Mogi M, Nakamura H, Horiuchi H, et al. Osteoprotegerin regulates bone formation through a coupling mechanism with bone resorption. Endocrinology 2003;144:5441–9.
[23] Cundy T, Hegde M, Naot D, Chong B, King A, Wallace R, et al. A mutation in the gene *TNFRSF11B* encoding osteoprotegerin causes an idiopathic hyperphosphatasia phenotype. Hum Mol Genet 2002;11:2119–27.
[24] Whyte MP, Obrecht SE, Finnegan PM, Jones JL, Podgornik MN, McAlister WH, et al. Osteoprotegerin deficiency and juvenile Paget's disease. N Engl J Med 2002;347:175–84.
[25] Chong B, Hegde M, Fawkner M, Simonet S, Cassinelli H, Coker M, et al. Idiopathic hyperphosphatasia and *TNFRSF11B* mutations: relationships between phenotype and genotype. J Bone Miner Res 2003;18:2095–104.
[26] Janssens K, de Vernejoul MC, de Freitas F, Vanhoenacker F, Van Hul W. An intermediate form of juvenile Paget's disease caused by a truncating *TNFRSF11B* mutation. Bone 2005;36:542–8.
[27] Cundy T, Davidson J, Rutland MD, Stewart C, DePaoli AM. Recombinant osteoprotegerin for juvenile Paget's disease. N Engl J Med 2005;353:918–23.
[28] Roodman GD, Windle JJ. Paget disease of bone. J Clin Invest 2005;115:200–8.
[29] Teufert KB, Linthicum Jr F. Paget disease and sensorineural hearing loss associated with spiral ligament degeneration. Otol Neurotol 2005;26:387–91.
[30] Huizing EH, de Groot JA. Densitometry of the cochlear capsule and correlation between bone density loss and bone conduction hearing loss in otosclerosis. Acta Otolaryngol 1987;103:464–8.
[31] Monsell EM. The mechanism of hearing loss in Paget's disease of bone. Laryngoscope 2004;114:598–606.
[32] Whyte MP, Hughes AE. Expansile skeletal hyperphosphatasia is caused by a 15-base pair tandem duplication in *TNFRSF11A* encoding RANK and is allelic to familial expansile osteolysis. J Bone Miner Res 2002;17:26–9.
[33] Hughes AE, Ralston SH, Marken J, Bell C, MacPherson H, Wallace RG, et al. Mutations in *TNFRSF11A*, affecting the signal peptide of RANK, cause familial expansile osteolysis. Nat Genet 2000;24:45–8.
[34] Zehnder AF, Kristiansen AG, Adams JC, Merchant SN, McKenna MJ. Osteoprotegerin in the inner ear may inhibit bone remodeling in the otic capsule. Laryngoscope 2005;115:172–7.
[35] Yano K, Tsuda E, Washida N, Kobayashi F, Goto M, Harada A, et al. Immunological characterization of circulating osteoprotegerin/osteoclastogenesis inhibitory factor: increased serum concentrations in postmenopausal women with osteoporosis. J Bone Miner Res 1999;14:518–27.
[36] Browner WS, Lui LY, Cummings SR. Associations of serum osteoprotegerin levels with diabetes, stroke, bone density, fractures, and mortality in elderly women. J Clin Endocrinol Metab 2001;86:631–7.
[37] Ueland T, Brixen K, Mosekilde L, Mosekilde L, Flyvbjerg A, Bollerslev J. Age-related changes in cortical bone content of insulin-like growth factor binding protein (IGFBP)-3, IGFBP-5, osteoprotegerin, and calcium in postmenopausal osteoporosis: a cross-sectional study. J Clin Endocrinol Metab 2003;88:1014–8.

ELSEVIER

Auris Nasus Larynx 34 (2007) 95–100

AURIS NASUS LARYNX
INTERNATIONAL JOURNAL OF ORL & HNS

www.elsevier.com/locate/anl

# Cholesterol granuloma surrounding the endolymphatic sac

Sho Kanzaki [a,b,*], Yasutomo Araki [a], Yasuhide Okamoto [a], Akihiro Kurita [a], Kaoru Ogawa [a]

[a] *Department of Otorhinolaryngology, School of Medicine, Keio University, 35 Shinanomachi, Shinjuku, Tokyo 160-8582, Japan*
[b] *Tokyo Electrical Power Company Hospital, Tokyo, Japan*

Received 18 January 2006; accepted 26 May 2006
Available online 17 August 2006

**Abstract**

We report a unique case of cholesterol granuloma (CG) surrounding the endolymphatic sac (ES). A 49-year-old man presented with the left side of sensorineural hearing loss, tinnitus, and vertigo. Magnetic resonance and computed tomography imaging revealed a CG surrounding the left ES. The patient initially underwent left transmastoid surgical resection of the tumor. At the time of surgery, brown fluid was aspirated from the tumor, but no other tumors were found. Histopathological examination revealed that the tumor contained cholesterol crystals, confirming the diagnosis of CG. At his 12-month postoperative follow-up, there was no evidence of recurrence. We discuss the radiology, pathology, and surgical removal of CGs surrounding ES.


*Keywords:* Cholesterol granuloma; Endolymphatic sac; Tumor; Surgery

## 1. Introduction

Endolymphatic sac (ES) is known as the neuroectodermally derived mucous membrane which lines the vestibular system of inner ear and is involved with resorption and production of endolymph. The tumor located in ES is very rare, but it is considered as endolymphatic sac tumor (ELST) which displays papillary adenoma or adenocarcinoma.

Cholesterol granuloma (CG) is containing fibrous and brownish-yellow fluid composed of globular material, lipids, and crystals [1]. CG is usually occurs in petrous apex or middle ear [1].

We have encountered a rare case of CG surrounding the ES. It was difficult to diagnose the tumor as CG before operation because CG and ELST similarly demonstrated high intensity of T1 weighted MRI findings.

Here, we report the radiological details of this case and describe the surgical approach we used to remove the CG.

## 2. Case report

A 49-year-old male that complained of left-sided hearing loss, tinnitus, and vertigo for 2 years was examined in Tokyo Electrical Power Company Hospital on January 19, 2004. Review of his history indicated that his symptoms progressively worsened. His previous doctor had initially suspected Meniere's disease and had prescribed a diuretic drug.

Upon our examination, there is normal finding in both sides of the tympanic membrane. Pure tone audiogram revealed a moderate sensorineural hearing loss on the left side (Fig. 1). When the patient shook his head, he exhibited right-directed horizontal and circular or rotary nystagmus, suggesting left side of inner ear damage. He did not display other complications beyond those related to the auditory syndrome.

Magnetic resonance imaging (MRI), performed to exclude cerebral and acoustic neurinoma, but showed an enhanced lesion surrounding the ES (Fig. 2A–C). Computed tomography (CT) was performed to assess mass extension and bone destruction (Fig. 2D).

* Corresponding author. Tel.: +81 3 3353 1211; fax: +81 3 3353 1261.
*E-mail address:* skan@sc.itc.keio.ac.jp (S. Kanzaki).

0385-8146/$ – see front matter © 2006 Published by Elsevier Ireland Ltd.
doi:10.1016/j.anl.2006.05.016

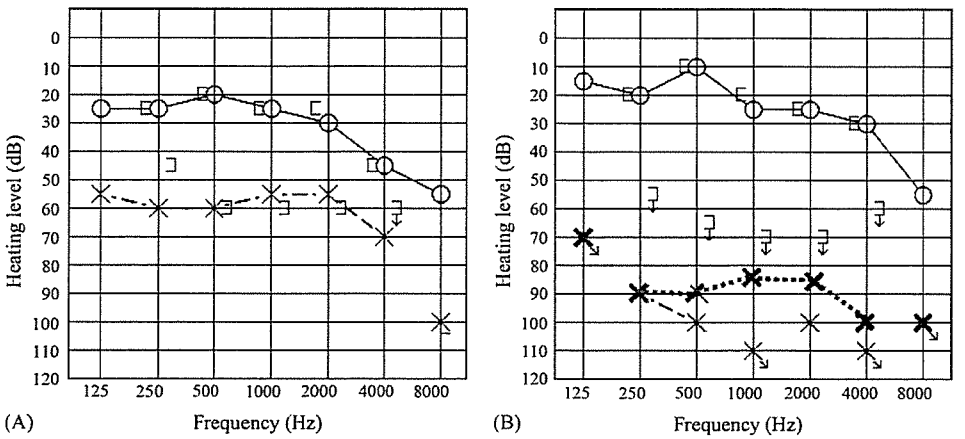


Fig. 1. Pure tone audiogram performed preoperatively (A) and 1 and 6 months postoperatively (B) revealed left-sided hearing loss. Audiograms measured from the left side (air conduction was shown as follows): thin dotted line (1 month), bold dotted line (6 months). The bone conduction has not changed between 1 and 6 month post-operation; Audiogram measured from the right side: solid line.

MRI demonstrated increased signal intensity on T1- and T2- (fluid inversion attenuated recovery; FLAIR) weighted images (Fig. 2A–C). Although these images were highly characteristic of CGs, we did not rule out the possibility of endolymphatic sac tumor (ELST). CT revealed bone destruction around the left ES and enlarged endolymphatic duct (ED) (Fig. 2D) but no compression of the internal auditory meatus. There was no serous effusion in the middle ear cavity. This tumor did not invade the cochlea and semicircular canals. The patient was subsequently moved to the Keio University Hospital for surgery.

After being admitted to the Keio University Hospital, this patient was subjected to several tests, including speech discrimination test, auditory brain stem response (ABR) test, and transient-evoked otoacoustic emission (TEOAE) and distorted product otoacoustic emissions (DPOAE) tests. The speech discrimination test revealed that the patient's speech reception threshold was 95% (60 dB) in the right ear and 65% (90 dB) in the left ear. ABR testing revealed that latency of wave I of the left ear (2.64 ms) was longer than that of the right ear (1.94 ms).

A low wave reproducibility and amplitude reduction were presented in TEOAE and significant response in DPOAE was not presented from the left ear (Fig. 3). Taken together, these audiologic findings suggested cochlear damage. Because symptoms associated with tumor-related compression of the ES are similar to those associated with Meniere's disease [2], we performed a preoperative glycerol test to rule out Meniere's disease. The glycerol test was negative, indicating that the pathologic lesion in this patient was probably not related to typical endolymphatic hydrops or Meniere's disease.

Transmastoid surgery was performed on April 28, 2004. We performed a mastoidectomy with the left side of retroauricular approach while the patient was under general anesthesia. Upon examination, the patient's sigmoid sinus and posterior cranial fossa appeared hypercalcified. Using diamond burs, we removed bone from the posterior fossa at the base of the sigmoid sinus, posteriorly from the sigmoid sinus and anteriorly behind the posterior semicircular canal, to expose bony aspects of the lateral and posterior semicircular canals. To gain access to the tumor, we drilled through the mastoid located behind the posterior semicircular canal. Once exposed, the wall of the CG was opened. Exudates were aspirated (Fig. 4). Following aspiration of the brown (chocolate like) fluid, part of the posterior fossa dura was exposed. We drained the pneumatic space and reestablished adequate aeration of the cavity. The posterior canals, ES, and ED were preserved (Fig. 4). During this time, excised tissue was examined using rapid histology methods and identified as granulation tissue. The mastoid cavity was not obliterated. Immediately after operation, the patient exhibited left-oriented horizontal and circular nystagmus for several hours. Neither meningitis nor facial palsy developed after operation.

Histopathological examination of the excised CG revealed cholesterol crystals, red blood cells and hemosiderin (Fig. 5). Indications of papillary adenoma or carcinoma were not present. The tissue exhibited negative S-100 staining which is a marker of ELST (data not shown). The final diagnosis was CG.

At 2 months after the operation, the left-sided hearing impairment worsened. However, the patient's hearing slightly improved at 6 months after operation. His vertigo disappeared and his hearing continued to improve (Fig. 1B). Caloric testing using 5 ml of 20 °C cold water demonstrated that maximum velocity of the slow phase was 26°/s in left side at 6 months after operation, suggesting that left side of vestibular function was not lost. However, we could not compare the caloric tests between pre- and post-operations because the patient did not want to have this test pre-operation. MRI has revealed no recurrences so far (Fig. 2E).

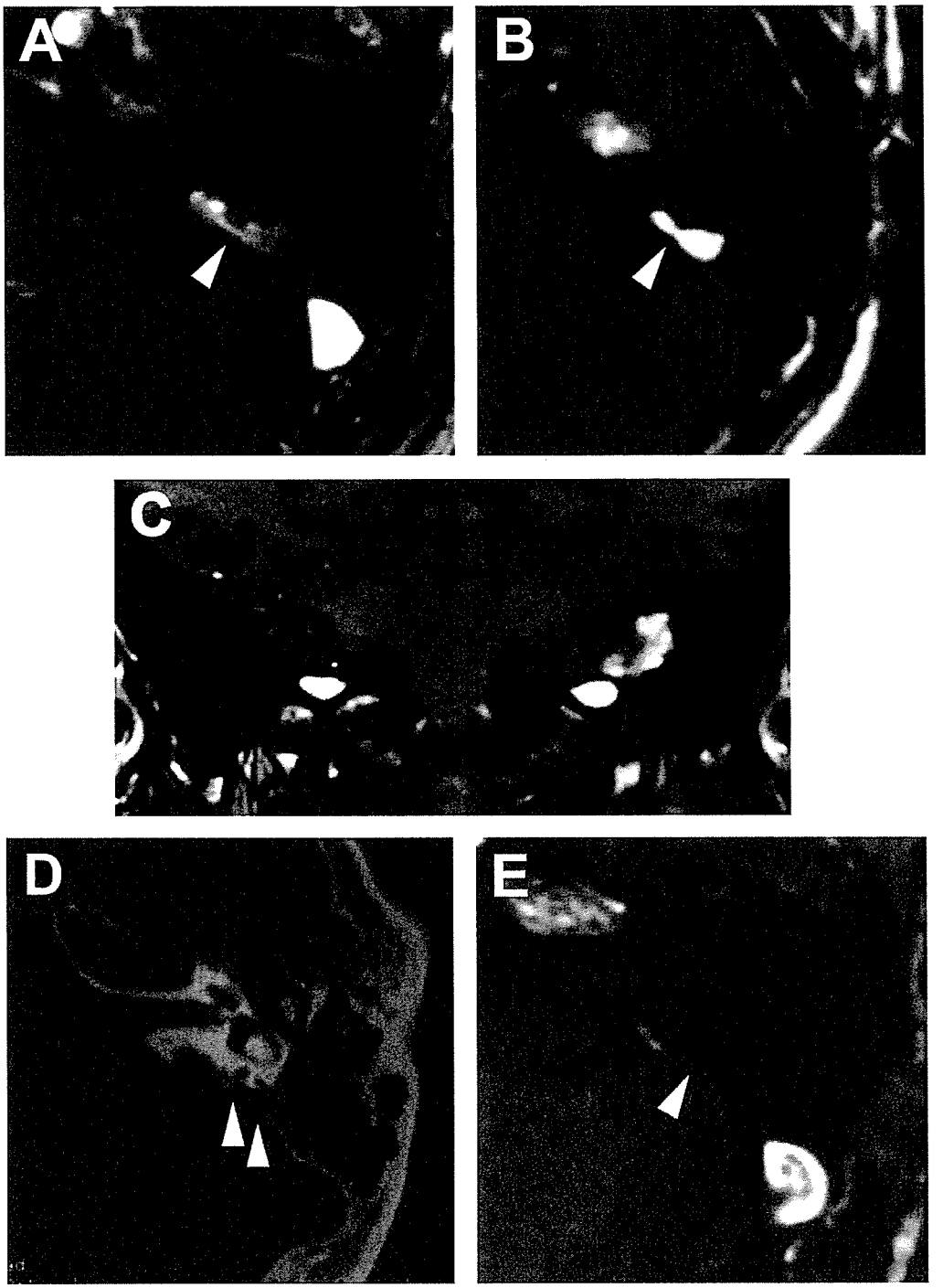


Fig. 2. Magnetic resonance (MR) and computed tomography (CT) images of the tumor. Axial T1-weighted (A) and T2-weighted with FLAIR (B) MRIs reveal a hyperintense cholesterol granuloma (CG) (arrowheads) adjacent to the endolymphatic sac. (C) Coronal T1-weighted MRI shows the CG (arrowhead) with heterogeneous signal intensity. (D) Axial CT shows the CG (arrowheads) abutting the endolymphatic sac. (E) Axial T2-weighted MRI taken 6 months after surgical resection of the CG mass. Recurrence of the CG is not apparent (arrowhead indicates the part surrounding ES).

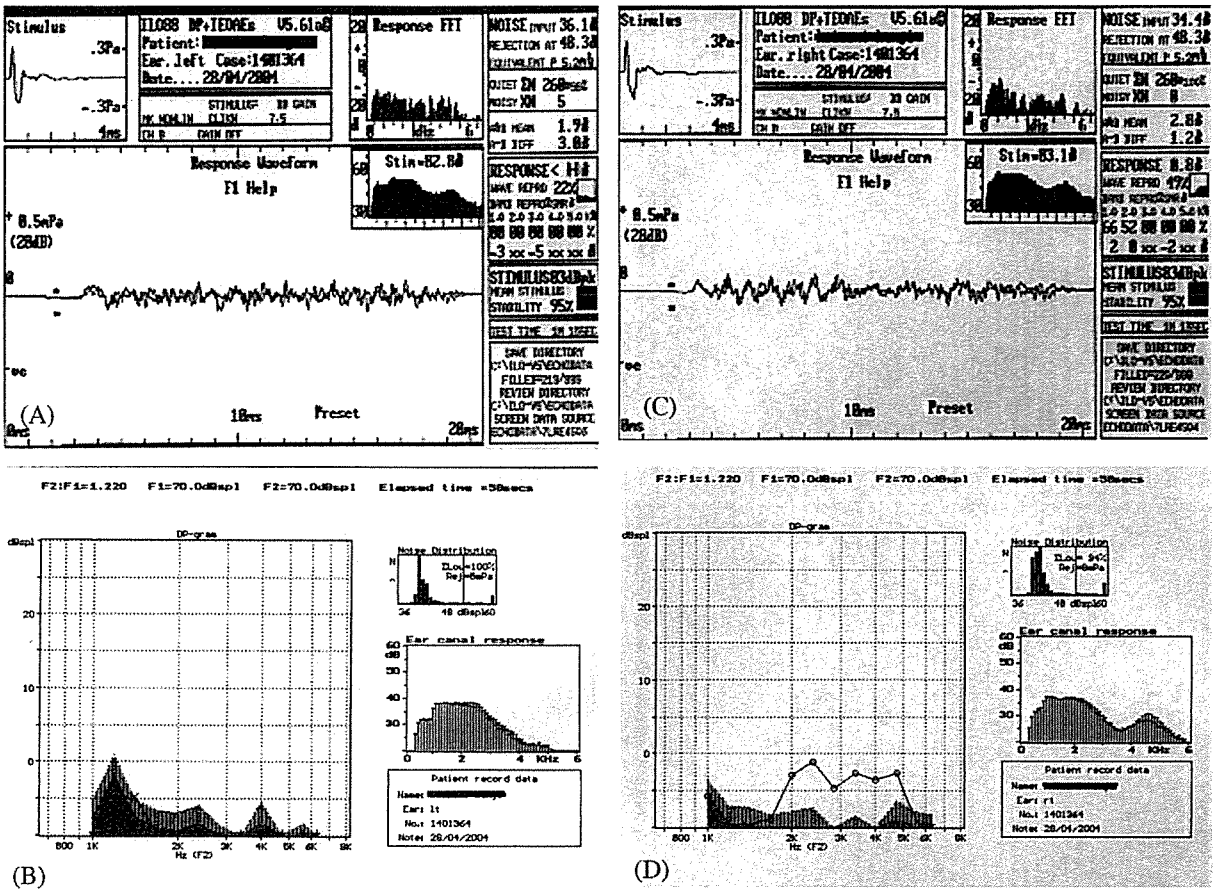


Fig. 3. Transient-evoked otoacoustic emission (TEOAE) and distorted product otoacoustic emission (DPOAE) measurements. (A and B) TEOAE. (C and D) DPOAE. Left ear (A and C) and right ear (B and D). There were no TEOAE and DPOAE responses from the left ear.

## 3. Discussion

This patient displayed symptoms characteristic of Meniere's disease, but had a CG surrounding the ES. The tumor surrounding ES is typically considered as ELST. CGs surrounding ES, as the one described in our case, is very rare. Although CGs can be generated anywhere in the temporal bone, CGs affecting anterior parts of the petrous apex occur typically [1].

The point of this case was differential diagnosis to distinguish CG from ELST at the pre-operation. In MRI, CGs typically exhibit high signal on T1- and T2-weighted images resulting from the paramagnetic effect of hemoglobin [3,4]. However, ELST lesions characteristically appear heterogeneous with scattered areas of signal and peripheral rim enhancement on T1-weighted images [5]. During the operation, we found fluid in the mastoid cells around the ES. We finally diagnosed the tumor as a CG because its histopathology revealed the presence of cholesterol crystals and several hemosiderin-containing macrophages but no papillary adenoma or adenocarcinoma. In addition, tumor demonstrated no S-100 specific staining which is one of the ELST markers [5] or neurogenic tumor.

Additionally, ELST includes sporadic ELST and ELST associated with von Hippel-Lindau (VHL) disease which is an autosomal dominant multisystem disorder [6]. Thus far, our patient remains free of such complications.

The etiology of this CG is unknown. There are two theories of etiology including classic and new theories. We speculated that the CG in this patient formed according to the classic theory of CG formation. That is, because the air cells within the petrous apex are convoluted and deeply embedded, they are difficult to aerate and drain in decreased atmospheric pressure, thus causing mastoid cells to hemorrhage. The subsequent catabolism of hemoglobin or breakdown of local tissues generates cholesterol, which in turn produces a "foreign body" or cell-mediated immune response [7–10]. On the other hand, a new theory proposed by Jackler and Cho demonstrated that CGs of the anterior petrous apex may arise from proclivous bone marrow and mucosa that ruptures, causing blood to pool within the anterior petrous apex [1]. However, this CG was not located in anterior petrous apex. This etiology may be different from new theory.

Hansen and Luxford described the surgical resections of 13 ELSTs and in their series one patient who had undergone transmastoid surgery for the resection of a presumed CG had

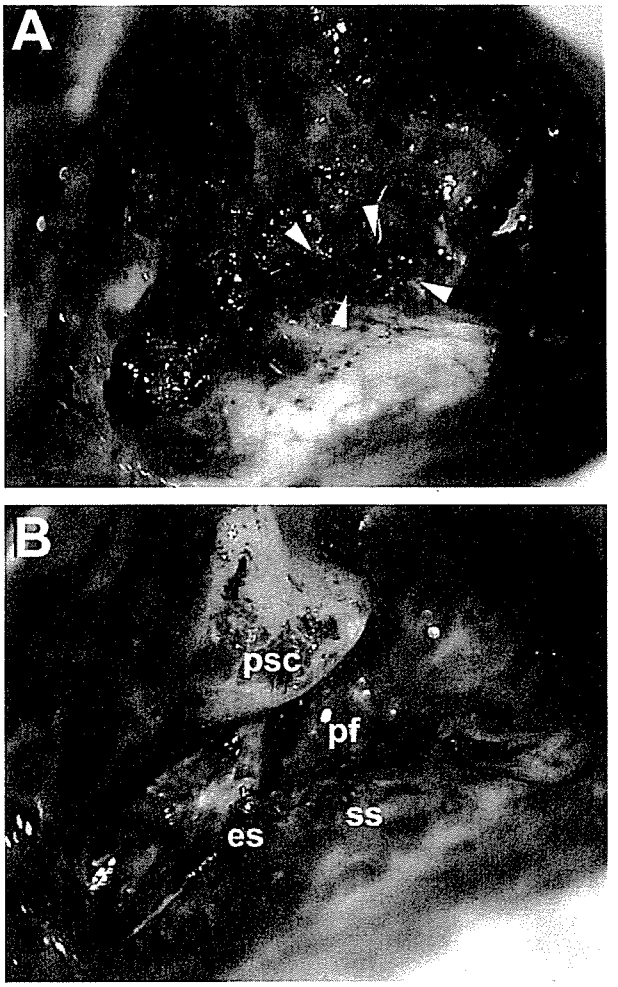


Fig. 4. Photograph of the operative field. (A) Arrowheads indicate wall of the cholesterol granuloma (CG). (B) Mastoid and endolymphatic sac after aspiration. *Abbreviations*: es, endolymphatic sac; psc, posterior semicircular canal; lsc, lateral semicircular canal; ss, sigmoid sinus; ps, posterior fossa.

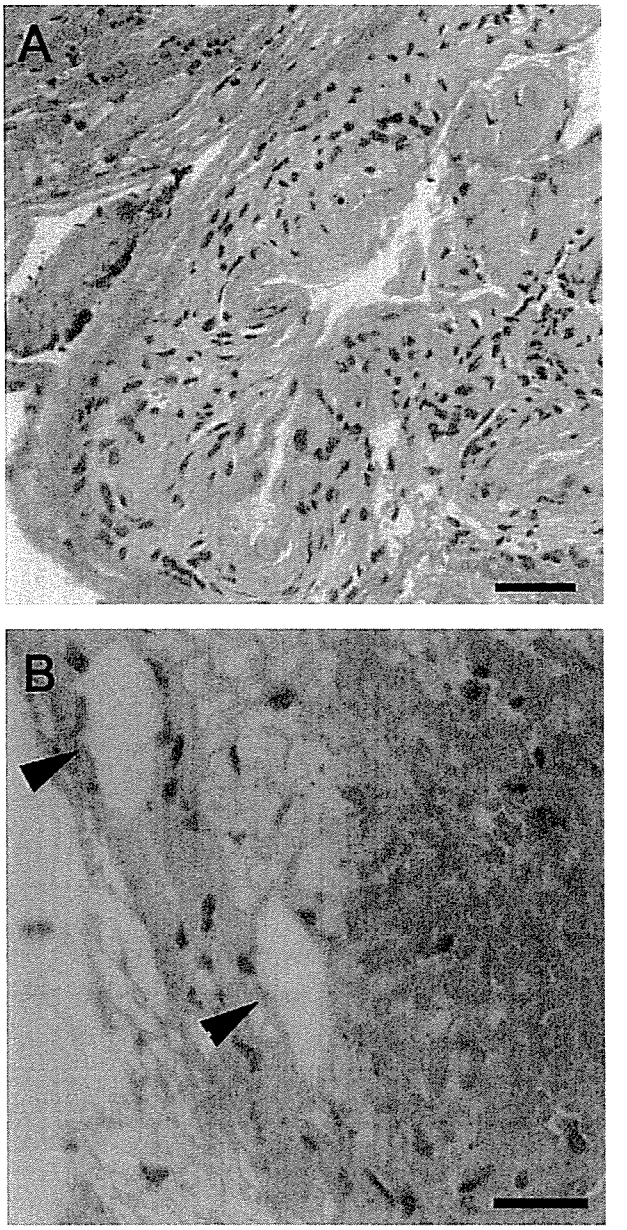


Fig. 5. Low (A) and high (B) magnification photomicrographs of a section through the excised cholesterol granuloma (CG) showing its histopathology. The CG mainly consisted of granulation tissue. A few cholesterol crystals (arrowheads) were also found. Scale bars: (A) 50 μm and (B) 15 μm.

a recurrence of the ELST 2 years after the initial operation [2]. This case might be also secondary CG followed by hemorrhage of small ELST although histological study has demonstrated granulation tissue so far. We need follow-up this case to detect the recurrence of tumor and occurrence of ELST. Therefore, a long-term follow-up (>24 months postoperative) of these patients is needed although MRI has not revealed the presence of ELSTs up to 12 months after surgery.

We discuss the correlation between the CG and Meniere's syndrome. Before the operation, the patient demonstrated negative in the glycerol test, which is often performed in suspected cases of Meniere's syndrome or hydrops. In humans, the ES of the inner ear have been suggested to control endolymph volume and homeostasis [11,12]. In most patients with endolymphatic hydrops, glycerol intake typically reduces endolymphatic fluid, but in our patient, endolymphatic fluid pressure remained unchanged because the CG supplied continuous pressure onto the ES. We speculated that the CG-associated pressure onto the ES induced the Meniere's syndrome-like symptoms in this patient. Because of these symptoms, it was difficult to determine preoperatively whether this pathology was hydrops. Indeed, it is often difficult to distinguish Meniere's syndrome from ELSTs on the sole basis of preoperative symptoms. Hansen and Luxford recently reported that only 3 of 14 ELST patients they examined actually had Meniere's syndrome [2]. ELSTs develop and press ES, inducing progressive hearing loss and repeated vertigo attacks [2]. Therefore, we speculated that CG in this case might develop after hemorrhage, pressed ES and then patients presented progressive symptoms.

Identification of small or in situ ELSTs offers patients to opt for the surgical removal of the tumors with the aim of hearing preservation [13]. Although we made a special effort to keep the ES intact during surgery, audiogram performed 2 months after surgery revealed that the patient's level of hearing was worse than preoperative levels. However, audiogram performed 12 months after surgery revealed that the patient's hearing has steadily improved but not to preoperative levels. In the present case, the patient's OAE response to stimuli was poor, thus, prompting us to speculate a poor prognosis for this patient in terms of postoperative recovery of hearing function. Additionally, the oscilation of drilling bone might result in ES, although ES macroscopically appeared intact.

In conclusion, we report the very rare case of a CG surrounding the ES. MRI was very useful for diagnosis. OAEs revealed the left-sided cochlear damage. Surgery was successful in draining the brown fluid from the CG mass. Vertigo and headache improved within 6 months after operation. Hearing function has recovered to some extent but not completely.

## References

[1] Jackler RK, Cho M. A new theory to explain the genesis of petrous apex cholesterol granuloma. Otol Neurotol 2003;24:96–106.
[2] Hansen MR, Luxford WM. Surgical outcomes in patients with endolymphatic sac tumors. Laryngoscope 2004;114:1470–4.
[3] Chang P, Fagan PA, Atlas MD, Roche J. Imaging destructive lesions of the petrous apex. Laryngoscope 1998;108:599–604.
[4] Kosling S, Bootz F. CT and MR imaging after middle ear surgery. Eur J Radiol 2001;40:113–8.
[5] Devaney KO, Ferlito A, Rinaldo A. Endolymphatic sac tumor (low-grade papillary adenocarcinoma) of the temporal bone. Acta Otolaryngol 2003;123:1022–6.
[6] Lonser RR, Kim HJ, Butman JA, Vortmeyer AO, Choo DI, Oldfield EH. Tumors of the endolymphatic sac in von Hippel-Lindau disease. N Engl J Med 2004;350:2481–6.
[7] Beaumont GD. The effects of exclusion of air from pneumatized bones. J Laryngol Otol 1966;80:236–49.
[8] Friedmann I. Epidermoid cholesteatoma and cholesterol granuloma; experimental and human. Ann Otol Rhinol Laryngol 1959;68:57–79.
[9] Main TS, Shimada T, Lim DJ. Experimental cholesterol granuloma. Arch Otolaryngol 1970;91:356–9.
[10] Goycoolea MV, Paparella MM, Juhn SK, Carpenter AM. Otitis media with perforation of the tympanic membrane: a longitudinal experimental study. Laryngoscope 1980;90:2037–45.
[11] Salt AN. Regulation of endolymphatic fluid volume. Ann N Y Acad Sci 2001;942:306–12.
[12] Couloigner V, Berrebi D, Teixeira M, Paris R, Florentin A, Bozorg Grayeli A, et al. Aquaporin-2 in the human endolymphatic sac. Acta Otolaryngol 2004;124:449–53.
[13] Megerian CA, Haynes DS, Poe DS, Choo DI, Keriakas TJ, Glasscock 3rd ME. Hearing preservation surgery for small endolymphatic sac tumors in patients with von Hippel-Lindau syndrome. Otol Neurotol 2002;23:378–87.

ARTICLE doi:10.1016/j.ymthe.2005.09.020

# Histopathological and Behavioral Improvement of Murine Mucopolysaccharidosis Type VII by Intracerebral Transplantation of Neural Stem Cells

Yasuyuki Fukuhara,[1,2] Xiao-Kang Li,[3] Yusuke Kitazawa,[3] Masumi Inagaki,[4] Kentaro Matsuoka,[5] Motomichi Kosuga,[1] Rika Kosaki,[1,2] Takuya Shimazaki,[6] Hitoshi Endo,[7] Akihiro Umezawa,[8] Hideyuki Okano,[6] Takao Takahashi,[2] and Torayuki Okuyama[1,2,*]

[1]*Department of Clinical Genetics and Molecular Medicine,* [3]*Department of Innovative Surgery,* [8]*Department of Reproductive Biology, and* [5]*Department of Pathology, National Center for Child Health and Development, 2-10-1 Okura, Setagaya-ku, Tokyo 157-8535, Japan*
[2]*Department of Pediatrics and* [6]*Department of Physiology, Keio University School of Medicine, 35 Shinanomachi, Shinjuku-ku, Tokyo 160-8582, Japan*
[4]*National Center of Neurology and Psychiatry, 1-7-1 Kounodai, Ichikawa-shi, Chiba 272-8516, Japan*
[7]*Biochemistry of Experimental Medicine, Jichi Medical School, Minamikawachi-machi, Kawachi-gun, Tochigi 329-0498, Japan*

**To whom correspondence and reprint requests should be addressed. Fax: +81 3 3416 2222. E-mail: okuyama-t@ncchd.go.jp.*

Available online 28 November 2005

**The therapeutic efficacy of neural stem cell transplantation for central nervous system (CNS) lesions in lysosomal storage disorders was explored using a murine model of mucopolysaccharidosis type VII (MPS VII). We used fetal neural stem cells derived from embryonic mouse striata and expanded *in vitro* by neurosphere formation as the source of graft materials. We transplanted neurospheres into the lateral ventricles of newborn MPS VII mice and found that donor cells migrated far beyond the site of injection within 24 h, and some of them could reach the olfactory bulb. A quantitative measurement indicated that the GUSB activity in the brain was 12.5 to 42.3% and 5.5 to 6.3% of normal activity at 24 h and 3 weeks after transplantation. In addition, histological analysis revealed a widespread decrease in lysosomal storage in the recipient's hippocampus, cortex, and ependyma. A functional assessment with novel-object recognition tests confirmed improvements in behavioral patterns. These results suggest that intracerebral transplantation of neural stem cells is feasible for treatment of CNS lesions associated with lysosomal storage disorders.**

**Key Words: neurosphere, mucopolysaccharidosis type VII, intracerebral transplantation**

## INTRODUCTION

Mucopolysaccharidosis type VII (MPS VII), or Sly syndrome, is a congenital lysosomal storage disorder (LSD) characterized by a systemic deficiency of β-glucuronidase (GUSB) activity [1]. This defect results in a progressive accumulation of undegraded glycosaminoglycans and subsequent lysosomal distension in multiple tissues, including the central nervous system (CNS). Enzyme replacement therapy and bone marrow transplantation are effective for correcting visceral manifestations of the disorder [2,3]. However, effective treatment of the CNS in patients with LSDs remains a major challenge.

With respect to cell therapy directed to the CNS in an MPS VII mouse, there are reports that the intracerebral transplantation of a genetically engineered neural progenitor [4] and retrovirally transduced syngeneic fibroblasts [5] corrected the lysosomal storage of the recipient's brain tissues. We also previously reported that adeno virally transduced rat amniotic epithelial cells injected into adult MPSVII mouse brains survived at the injection point for more than 9 weeks and the subsequent supply of enzyme resulted in pathological improvement in multiple areas of the MPS VII mouse brains [6].

In this study, we used fetal neural stem cells derived from embryonic mouse striata and expanded *in vitro* by neurosphere formation [7,8] as the source of graft materials. Neural stem cells are considered to be good candidates for cell therapy to treat CNS dysfunction. In fact, fetal neural tissues have been successfully used in human Parkinson disease patients [9,10]; however, as many as four to eight fetuses were required to obtain a sufficient number of cells to treat a single patient. Expansion of neural stem cells *in vitro* may overcome the above practical

*Abbreviations used:* CNS, central nervous system; GUSB, β-glucuronidase; MPS VII, mucopolysaccharidosis type VII.



1525-0016/$30.00

and ethical problems associated with fetal tissue transplantation and provide a source for graft material.

Here we describe improvements in the histopathology of the hippocampus, cortex, and ependyma and in nonspatial hippocampus-dependent learning and memory evaluated in a novel-object recognition test at 2 months after transplantation. These data suggest that early transplantation of neurospheres into the CNS may prevent or delay some of the progressive mental impairment associated with this LSD.

## Results and Discussion

### Production and Secretion Capacity of GUSB Enzymes by Neurospheres

The neurosphere is a floating cell cluster containing plenty of neural stem cells and is generated from a fetal mouse brain by neurosphere formation [7,8]. Briefly, when we culture fetal corpus striatum containing neural stem cells in a serum-free medium with growth factors, only neural stem cells can survive and form floating cell clusters called neurospheres. We initially determined the endogenous GUSB activity of neurospheres obtained from normal C57BL/6 mice. The GUSB activity of the neurosphere and its culture medium proved significantly higher than that of bone marrow cells (Figs. 1A and 1B). We also evaluated the difference in GUSB activity before and after differentiation. Most neurospheres differentiate into neural cells *in vivo* according to their microenvironments after transplantation [8]. The GUSB activities in differentiated cells and their culture media were almost equivalent to those of bone marrow cells, suggesting that the GUSB activity of the neurospheres was reduced, although it was maintained to the extent necessary for a therapeutic effect even after differentiation.

### Intercellular Transport of the GUSB Enzyme

It is well known that most lysosomal enzymes can be taken up into cells by M6P receptor-mediated endocytosis, and that this process is efficiently blocked in the presence of M6P [11]. When we transferred the culture medium of neurospheres generated from C57BL/6 fetal mouse brains to dishes of the primary culture of neurons generated from C3H mice, 21.9% of the heat-stable C57BL/6 mouse-derived GUSB in the culture medium was internalized into the neurons in the absence of M6P (Fig. 1C). In contrast, it was significantly reduced in the presence of 10 mM M6P (Fig. 1C). This suggests that endocytosis by M6P receptors leads to the internalization of the GUSB enzyme secreted from the neurospheres to the neurons.

### Lysosomal Enzyme Activities of the Neurosphere

Many LSDs display CNS symptoms. Most lysosomal enzymes have common transport systems mediated by the M6P receptor, and therefore the same transplantation strategy could be available if neurospheres can produce and secrete significant amounts of lysosomal enzymes. We determined the specific activities of several lysosomal enzymes in neurospheres and compared them with those in marrow stromal cells and human granulocytes. Similar or higher activities of lysosomal enzymes were identified in the neurosphere (Table 1).

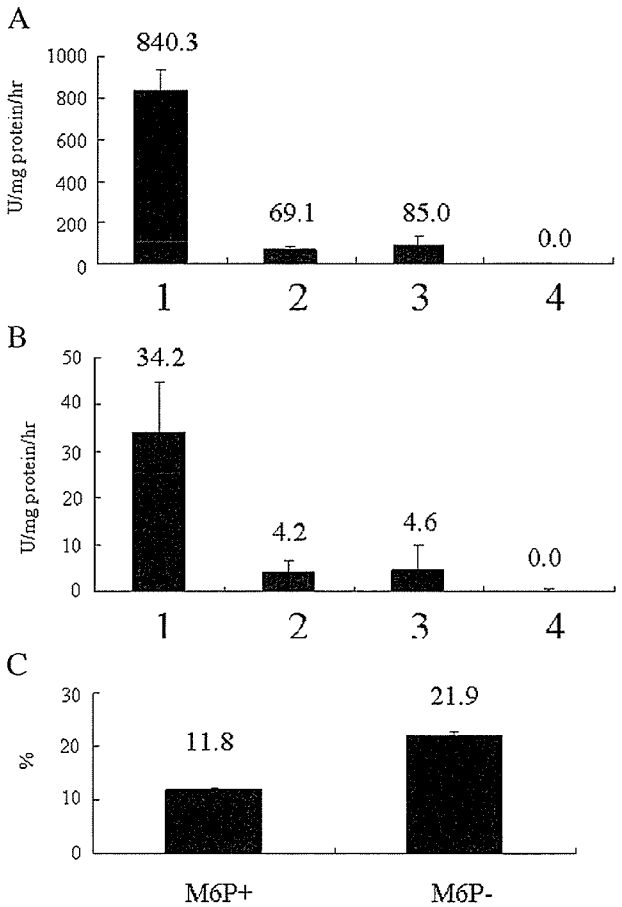


FIG. 1. Neurosphere GUSB activities and secretion via cell-to-cell transport. Lanes 1, neurospheres; 2, differentiated cells from neurospheres; 3, bone marrow cells; 4, 3521 cells (fibroblasts that originated from an MPS VII mouse). The GUSB activities of the neurosphere and its culture medium proved significantly higher than those of bone marrow cells. The GUSB activity in differentiated cells from neurospheres and that of its culture medium were almost equivalent to those of bone marrow cells. (A) GUSB activity in cell pellets of the neurosphere, bone marrow, and 3521 cells. (B) GUSB activity in a culture medium of the neurosphere, bone marrow, and 3521 cells at the time of the first passage. (C) Cell-to-cell transport of GUSB secreted from neurospheres. The ratio of the heat-stable GUSB activity in C3H mouse neural cells to the total heat-stable GUSB activity in the culture medium was calculated. The means ± standard errors are provided.

### Distribution of Donor Cells after Neonatal Transplantation

We performed a syngeneic transplantation experiment using neurospheres obtained from CAG-EGFP transgenic

doi:10.1016/j.ymthe.2005.09.020

**TABLE 1:** Activities of lysosomal enzymes in the neurosphere and their related diseases[a]

| Lysosomal enzyme | Disease | Neurosphere | MSC[b] | Granulocytes |
|---|---|---|---|---|
| α-L-Iduronidase | MPS I | 39.2 | 57.4 | 56–201 ($n$ = 6) |
| Iduronate sulfatase | MPS II | 40.5 | 20 | 12–26 ($n$ = 5) |
| Heparan-*N*-sulfatase | MPS IIIA | 1.1 | 4.3 | 0.2–3 ($n$ = 4) |
| GalNAc-6-*S*-sulfatase | MPS IVA | 5.3 | 15.2 | 8.1–20 ($n$ = 5) |
| Arylsulfatase B | MPS VI | 55.3 | 15.5 | 9–32 ($n$ = 5) |
| β-Glucosidase | Gaucher disease | 3.0 | 6.5 | 0.2–0.6 ($n$ = 100) |
| α-Galactosidase A | Fabry disease | 189 | 68.8 | 49.8–116.4 ($n$ = 48) |
| β-Galactosidase | MPS IVB | 501 | 309 | 37.6–230.1 ($n$ = 100) |
| α-Mannosidase | α-Mannosidosis | 61.0 | 48.0 | 121.1–345.1 ($n$ = 100) |
| β-Hexosaminidase | Sandhoff disease | 1024 | 3062 | 401.7–1426.0 ($n$ = 100) |
| β-Hexosaminidase A | Tay–Sachs disease | 527 | 481 | 251.1–607.4 ($n$ = 48) |
| Arylsulfatase A | MLD | 435 | 278 | 109.0–217.2 ($n$ = 100) |

[a] We quantitatively assayed for a variety of lysosomal enzymes as well as GUSB. Several kinds of lysosomal enzymes were found to be high in the neurosphere. This result suggests that the neurosphere may be applied for the treatment of different types of congenital metabolic disorder. Data are given in nmol/mg protein/h. Enzyme activities in human granulocytes were measured as described elsewhere [27].
[b] MSC, marrow stromal cell.

mice (C57BL/6 background) as donor cells and newborn MPS VII mice as recipients. We injected 2.5–5 × $10^4$ neurospheres (Fig. 2A) into the lateral ventricles of neonatal MPS VII mice within 1 to 3 days after delivery. A large number of donor cells were located mainly in the periventricular area at the hippocampus level in the brain, but a small number of GFP-positive cells were observed at varying distances away from the periventricular area at 24 h (Fig. 2B). We identified some of the GFP-positive cells in a linear formation at the level of the olfactory bulb, indicating a specific manner of migration in this area that is referred to as chain migration [12] (Fig. 2C). The overall distribution of the donor cells throughout the brain was essentially identical in all mice examined histologically ($n$ = 3), with findings similar to previous reports [4,13–15]. There was evidence of GUSB

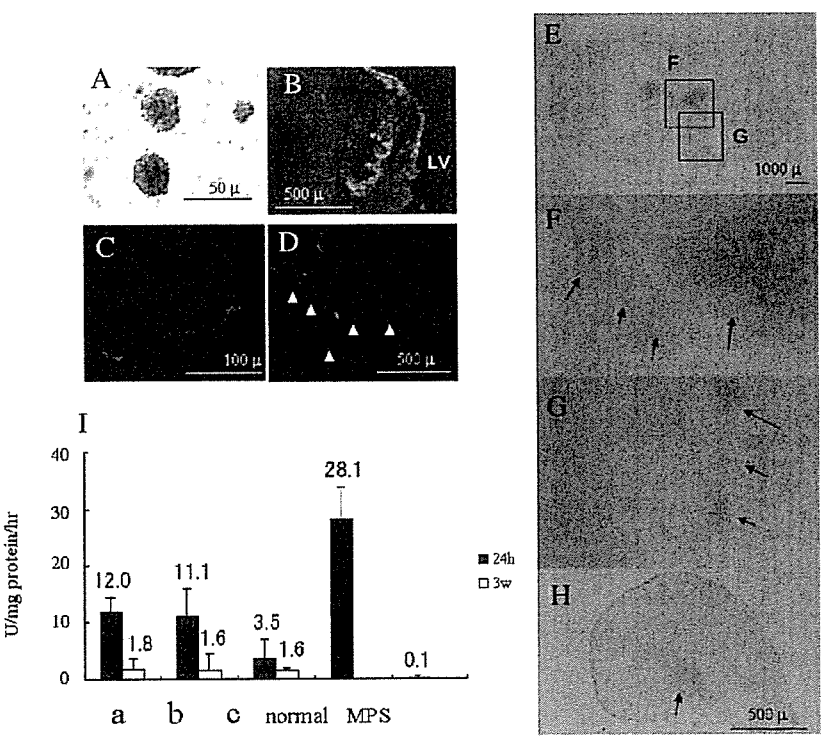


FIG. 2. Distribution of the donor cells in a mouse brain following transplantation of neurospheres. (A) Neurospheres generated from GFP transgenic mice under a fluorescence microscope. (B) A slice at the hippocampus level in the brain at 24 h after transplantation under a fluorescence microscope. GFP-positive cells were located mainly in the periventricular area. (C) A slice at the olfactory bulb level in the brain at 24 h after transplantation. GFP-positive cells were also detected under a fluorescence microscope; some of them were found to form a line (a chain migration). (D) A slice at the hippocampus level in the brain under a fluorescence microscope at 3 weeks after transplantation. GFP-positive cells were found to be branched and to form a network with the recipient brain tissue. (E–H) The brain of an MPS VII mouse at 24 h after transplantation of neurospheres. The recipient brain was stained red by GUSB staining in accordance with the GFP-positive area. (E–G) Coronal sections of the telencephalon at the caudal level. (H) Olfactory bulb. (I) Quantitative determination of the GUSB activity was performed at 24 h and 3 weeks after transplantation. The brains of the transplant recipients were divided coronally into three parts and quantitatively assayed for GUSB activity ($n$ = 3). The regions used for evaluation at the designated times were defined by anatomical landmarks in the anterior-to-posterior plane: a, olfactory bulbs; b, caudal edge of the olfactory bulbs to the rostral edge of the hippocampus; c, hippocampus to the posterior colliculus. The cerebellum was dissected free and was not included in the assay.

staining in accordance with the GFP-positive area, indicating a rise in GUSB activity (Figs. 2E–2H).

We previously reported that neurosphere-derived donor neurons extend their processes into the host tissues and form a synaptic structure [8]. The GFP-positive cells had extended their processes and formed synaptic structures as well 3 weeks after transplantation (Fig. 2D). These data suggest that the donor cells migrated from the periventricular area and some of them reached the olfactory bulb as early as 24 h after transplantation.

### Quantitative Gusb Assay in Transplanted Mouse Brains

We divided the brains of the transplant recipients coronally into three parts and quantitatively assayed them for GUSB activity at 24 h ($n$ = 3) and 3 weeks ($n$ = 3) after transplantation (Fig. 2I). GUSB activity was 12.5 to 42.3% of normal activity at 24 h. There was 5.5 to 6.3% of normal activity at 3 weeks after transplantation. This is an amount at which that lysosomal distensions in the neuron and glia could also be reversed [16]. These results imply that donor cells provided the recipient brain with GUSB activity to the extent that lysosomal storage in the recipient brain could be prevented for at least 3 weeks.

### Histological Analysis and Tumorigenesis Assessment of the Treated Mice

We tested the treated MPS VII mice for reduction of lysosomal distensions in the neurons and glia at 2 months after transplantation ($n$ = 2) (Figs. 3 and 4). We performed a histological analysis on hippocampus, cortex, and ependyma using an optical microscope (hippocampus, cortex, and ependyma) and an electron microscope (cortex). In the hippocampus of the untreated MPS VII mice, most of neurons contained marked cytoplasmic vacuolation (lysosomal storage) as well as astrocytes. In contrast, those of the treated hippocampuses were almost eliminated especially from neurons in this area. In the cortices, we also observed extensive neuronal and glial vacuolation, and the treatment reduced them remarkably as well. An electron microscope demonstrated that lysosomal storage in some neurons was completely eliminated in this area

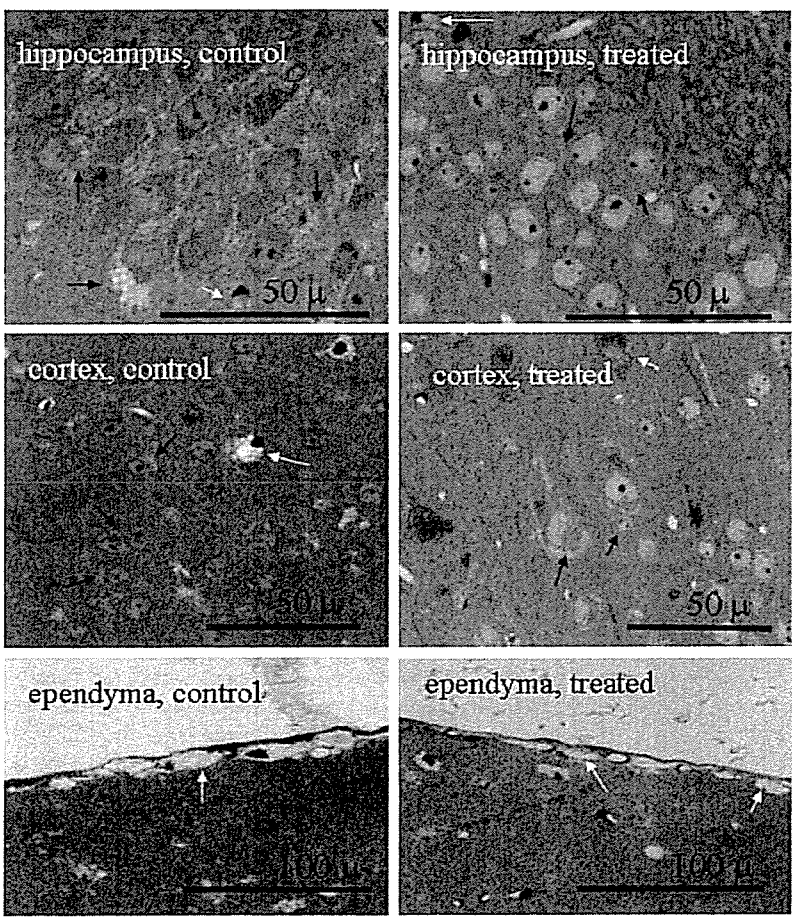


FIG. 3. Toluidine blue-stained, 0.5-μm-thick sections from the hippocampus, cortex, and ependyma are from 2-month-old MPS VII mice ($n$ = 2). Intraventricular injection of neurospheres decreases lysosomal storage in the hippocampus, cortex, and ependyma. Black arrows indicate distended vacuoles in neurons; white arrows indicate storage in glia.

doi:10.1016/j.ymthe.2005.09.020

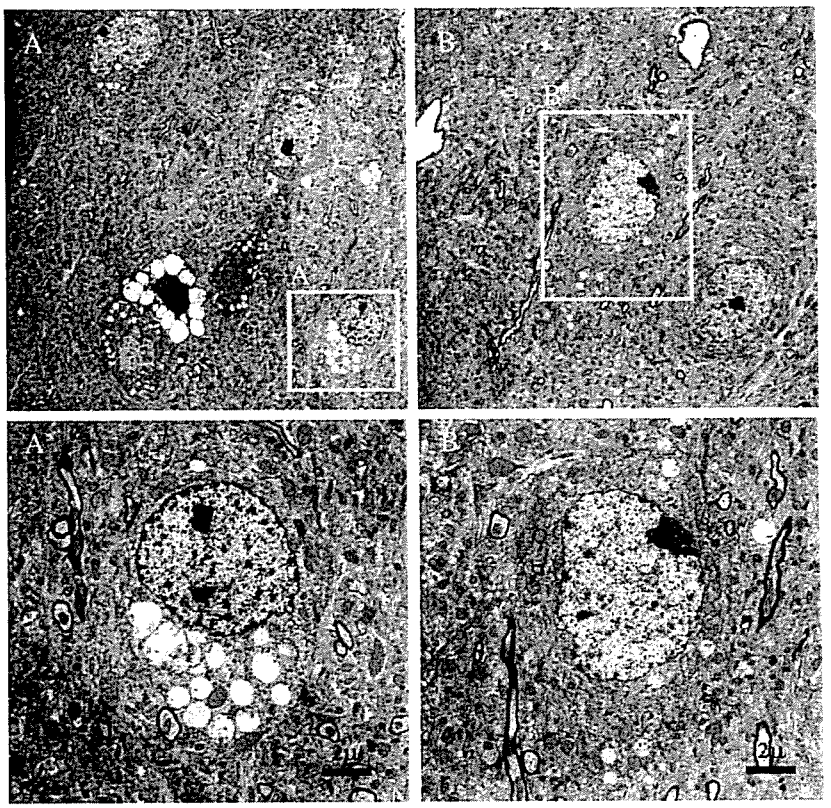


FIG. 4. Electron microscopic analysis of lysosomal storage in a mouse brain following transplantation of neurospheres. (A) Cortex of a control untreated MPS VII mouse at 2 months after transplantation. Abundant white cytoplasmic vacuoles represent distended lysosomes. (B) Cortex of a MPS VII mouse at 2 months after transplantation. Lysosomal storage granules in this area were remarkably reduced in size and number, and those in some neurons were completely eliminated. (A' and B') Magnified photographs of the circumscribed areas in (A) and (B).

(Fig. 4). In the ependyma, the amount of storage appeared to be significantly reduced in the treated mice. To evaluate quantitatively the improvement of the pathology in the treated mice, we counted neurons and glia containing apparent vacuolation in each hippocampus and cortex of the treated and the untreated mice ($n = 2$, total 300 cells in each area) in the HPF (×600). In both areas, we observed a remarkable decrease in the number of neurons and glia with apparent lysosomal storage, and this finding was almost equal in two treated mice, indicating an improvement of the pathology in the treated mouse brains (Table 2). We carefully assessed all transplanted mice for the presence of tumorigenesis. We dissected the brains of the dead mice during the course of the study and macroscopically analyzed them for tumor formation, but we could not identify any tumor formation among them.

**TABLE 2:** The percentage of cells with apparent vacuolization in the brain of MPS VII mice treated with intraventricular injection of neurospheres[a] ($n = 2$)

| | Untreated | Treated |
|---|---|---|
| Hippocampus | 89.3% | 17.3% |
| Neuron | 90% | 18.4% |
| Glia | 92% | 13.9% |
| Cortex | 42% | 15.3% |
| Neuron | 37.7% | 11.7% |
| Glia | 55.6% | 30% |

[a] Toluidine blue sections of hippocampus and cortex were analyzed for lysosomal distention, and we counted neurons and glia containing much vacuolation in 300 cells in each of hippocampus and cortex in the HPF (×600).

### Mouse Hearing Acuity Assessment

Measurements of the auditory brain-stem response (ABR) have been useful in assessing functional improvements after treatment [17]. We tested three treated MPS VII mice, three untreated MPS VII mice, and three C57BL/6 mice. There was no significant difference in the ABR thresholds among the treated and the untreated MPS VII mice (Fig. 5A). It is well known that malalignment and focal loss of stereocilia occur as the disease progresses, leading to a sensorineural hearing loss [18]. As the ABR was performed at 2 months, it may have been too early to assess the sensorineural hearing loss.

### Behavioral Assessment

We used a novel-object recognition test, a tool for studying nonspatial hippocampus-dependent memory, to determine whether an improvement in mental status could be achieved by transplantation [19–21]. We carried out this test as described [19] with several modifications at 2 months after transplantation ($n = 3$). We used normal siblings of the treated MPS VII mice as the control mice. In summary, after the mice were habituated to an open field, two yellow objects (A, B) were placed diagonally in

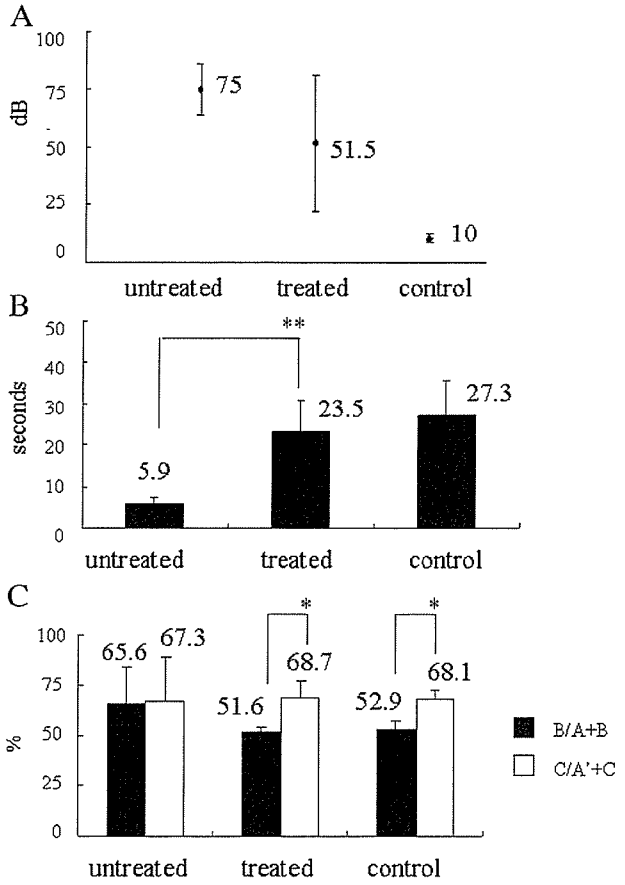


FIG. 5. Assessment of the functional recovery at 2 months after transplantation. (A) Auditory-evoked brain-stem responses. The decibels required to elicit ABR at the broadband (clicks) were evaluated among three normal mice, three treated MPS VII mice, and three untreated MPS VII mice at 2 months after transplantation. There was no significant difference in the ABR thresholds among the treated MPS VII mice and the untreated MPS VII mice. (B) The novel-object recognition test. The mice were assessed for an improvement in hippocampus-dependent nonspatial memory by a novel-object recognition test ($n = 3$). The total time spent exploring objects on day 4 (=A + B) in the treated mice was significantly longer than that for the untreated mice. (**$P < 0.01$). (C) The novel-object recognition test (retention test). The percentage of time spent in exploring B as a portion of the total object exploration time on day 4 [B/(A + B)] was compared with that of C (the novel object) on day 5 [C/(A′ + C)]. C/(A′ + C) in the C57BL/6 and the treated mice was significantly greater than B/(A + B). This suggests that the normal mice and the treated mice spent a significantly longer time exploring the novel object, revealing that both groups had a significant preference for exploring the novel object. The means ± standard errors are provided.

the open field on day 4, and the mice were allowed to explore them for 10 min. Object B was replaced with a novel object (C) and the other object was replaced with a replica (A′) on day 5, and the mice were again allowed to explore them for 10 min. Normal animals prefer to explore the novel object more than the familiar object. From the degree of preference for exploration of the new object, it can be inferred that they retained a memory of the familiar object. The total time spent exploring object A or B on day 4 (=A + B) was 27.3 ± 8.4 s in the normal mice, 23.5 ± 7.4 s in the treated mice, and 5.9 ± 1.6 s in the untreated mice (Fig. 5B), indicating that the normal and the treated mice had the same levels of motivation, curiosity, and interest in exploring objects. Next, to evaluate preferential exploration of the novel object, we compared the percentage of time spent exploring object B as a portion of the total object-exploration time on day 4 [=B/(A + B)] with that of object C (the novel object) on day 5 [=C/(A′ + C)] (Fig. 5C). C/(A′ + C) in the normal and the treated mice was significantly greater than B/(A + B) [normal mice, B/(A + B) = 52.9 ± 3.9%, C/(A′ + C) = 68.1 ± 4.4%; treated mice, B/(A + B) = 51.6 ± 2.8%, C/(A′ + C) = 68.7 ± 8.4% of the exploration time]. This indicates that the normal mice and the treated mice spent a significantly longer time exploring the novel object, revealing that both groups exhibited a significant preference for exploring it. These results indicate that the treated mice have the same level of nonspatial hippocampus-dependent memory as the normal mice. But we cannot completely deny the possibility that the vision had an influence on this improvement of a novel object test.

To date, there are reports demonstrating an improvement in behavior of treated MPS VII mice assessed by a Morris water maze test [22,23]. We used a novel-object test because it is very easy and less of a burden on the mice than the Water maze test. Consequently, it is easily applicable to mice with motility disturbance, and we thought we could maximize mouse performance associated with visual recognition memory. The long-term effects of this treatment have not been examined in detail. The treated mice lived to 7 months of age at most. Transplantation of neurospheres did not extend the life span of MPS VII mice. Life span may be dependent on systemic lysosomal storage other than the CNS.

In summary, our results demonstrated that after transplantation of *in vitro*-expanded neurospheres into the neonatal ventricle of MPS VII mice brains, the transplant donor cells migrated along established routes and integrated into the recipient's brain. The treated mice exhibited improved cognitive functions as measured by a novel-object recognition test, which was consistent with histological evidence of reduced lysosomal storage in the brain tissue.

## Materials and Methods

***Animals.*** Syngeneic MPS VII (*mps/mps*) mice were obtained from a pedigree colony of B6.C-H-2$^{bm1}$/ByBir-gus$^{mps}$/+ mice maintained at our facility [6]. Normal C3H mice were purchased from Shizuoka Laboratory Animal Center (Shizuoka, Japan). CAG-EGFP transgenic mice were originally generated by Endo *et al.* [24,25]. All mice were maintained and treated in accordance with the guidelines of the animal committee of the facility.

***Isolation, primary cultures, and passaging procedures of neurospheres.*** Embryos were removed from CAG-EGFP transgenic mice on day 14.5 of pregnancy. The corpus striatum was dissected and prepared as described

doi:10.1016/j.ymthe.2005.09.020

elsewhere [7]. Neurospheres were cultured in the medium described below at 37°C with 5% $CO_2$ at a concentration of $2 \times 10^5$ cells/ml in the primary culture. The culture medium was DMEM/F12 supplemented with the hormone mixture used by Reynolds and Weiss [7]. Passages were performed once per week. Neurospheres were used for the transplantation after the second to fifth passage.

***Cell-to-cell transport of GUSB secreted from neurospheres.*** We evaluated *in vitro* the uptake ratio of the GUSB enzyme secreted from neurospheres of C57BL/6 mice into neural cells of C3H mice by using the difference in the heat stability of GUSB proteins between C57BL/6 mice and C3H mice. In brief, GUSB activity of C57BL/6 mice was reduced by only 30% after a 2-h incubation at 65°C [11]. In contrast, GUSB activity of C3H mice was decreased markedly after this procedure. We prepared a culture medium of neurospheres from C57BL/6 mice after 1 week incubation. We replaced the medium of primary neurons of C3H mice with the above medium, continued to culture in the presence or absence of M6P, and harvested 12 h later. Heat-stable GUSB activity in the homogenates of C3H mouse neurons was measured after a 2-h incubation at 65°C.

***Quantitative analysis of GUSB activity.*** GUSB activity in tissues and cell homogenates was quantified using a fluorometric assay described previously [26]. Neurospheres were quantitatively analyzed after the second to fifth passage. Differentiated cells were obtained from neurospheres by converting the culture medium into DMEM +10% FBS. We had previously demonstrated that these cells differentiated into neurons, astrocytes, and oligodendrocytes by immunological staining (data not shown). Bone marrow was isolated from C57BL/6 mice and cultured in DMEM +10% FBS. Attached cells were collected after the second to fifth passage and analyzed for GUSB activity.

***Histochemical detection of GUSB activity.*** The mice were perfused with physiological saline and subsequently with 4% paraformaldehyde before preparation of the brains. The brains were equilibrated in a 30% sucrose solution (4°C, overnight), frozen in M-1 embedding matrix (Shandon, Pittsburgh, PA, USA), and then sectioned on a cryostat. Histochemical analysis of GUSB activity was performed on 20-μm-thick frozen sections using naphthol AS-BI β-D-glucuronide (Sigma) as a substrate [26].

***Lysosomal enzyme activities of the neurosphere.*** Lysosomal enzyme activities in neurospheres, the marrow stromal cells, and human granulocytes were quantified using a fluorometric assay as described with some modification [27].

***Histopathological analysis of lysosomal storage.*** Histopathology in neurons and glia was analyzed at 2 months after transplantation, corresponding to 2 months of age ($n = 2$). Tissues were isolated from the mice and immediately immersed in cold 2% glutaraldehyde in 0.1 M cacodylate buffer, postfixed in 1% osmium tetroxide, dehydrated through a graded series of ethanol solutions, and embedded in Spurr's Medium (Polyscience, Warrington, PA, USA). Toluidine blue-stained, 0.5-μm-thick sections were analyzed for evidence of lysosomal storage in hippocampus, cortex, and ependyma. Cytoplasmic lysosomal distensions in the cortex were also evaluated with an electron microscope.

***Auditory brain-stem responses.*** ABR examination was performed 20 min after anesthesia in a quiet room, as described previously [28].

***Novel-object recognition tests.*** Novel-object recognition tests evaluate nonspatial hippocampus-dependent learning and memory [19–21] and were performed as described [19] with several modifications. The mice were habituated in an open field over a 2-day preexposure (day 1 for 5 min and day 3 for 5 min). Two yellow objects (A and B) were placed diagonally in the open field (15 cm away from the walls) on day 4, and the mice were allowed to explore them for 10 min. Object B was replaced with the novel object (C), and the other object was replaced with a replica (A′) on day 5, and the mice were again allowed to explore them for 10 min. Recognition of the familiar object was scored by preferential exploration of the novel object. A + B represents total time exploring on day 4. A′ + C represents total time exploring on day 5. B/(A + B) represents the ratio of time exploring object B to total time exploring on day 4. C/(A′ + C) represents the ratio of time exploring object C to total time exploring on day 5.

## ACKNOWLEDGMENTS

*This work was supported by a grant from Terumo Foundation Life Science Foundation to HO, and a grant from the 21st Century COE program of the Japanese Ministry of Education, Culture, Sports, Science and Technology Ministry to Keio University.*

RECEIVED FOR PUBLICATION APRIL 27, 2005; REVISED SEPTEMBER 13, 2005; ACCEPTED SEPTEMBER 27, 2005.

## REFERENCES

1. Sly, W. S., Quinton, B. A., McAllister, W. H., and Rimoin, D. L. (1973). β-Glucuronidase deficiency: report of clinical, radiologic, and biochemical features of a new mucopolysaccharidosis. *J. Pediatr.* **82:** 249–257.
2. Vogler, C., *et al.* (1993). Enzyme replacement with recombinant beta-glucuronidase in the newborn mucopolysaccharidosis type VII mouse. *Pediatr. Res.* **34:** 837–840.
3. Birkenmeier, E. H., *et al.* (1991). Increased life span and correction of metabolic defects in murine mucopolysaccharidosis type VII after syngeneic bone marrow transplantation. *Blood* **78:** 3081–3092.
4. Snyder, E. Y., Taylor, R. M., and Wolfe, J. H. (1995). Neural progenitor cell engraftment corrects lysosomal storage throughout the MPS VII mouse brain. *Nature* **374:** 367–370.
5. Taylor, R. M., and Wolfe, J. H. (1997). Decreased lysosomal storage in the adult MPS VII mouse brain in the vicinity of grafts of retroviral vector-corrected fibroblasts secreting high levels of β-glucuronidase. *Nat. Med.* **3:** 771–775.
6. Kosuga, M., *et al.* (2001). Engraftment of genetically engineered amniotic epithelial cells corrects lysosomal storage in multiple areas of the brain in mucopolysaccharidosis type VII mice. *Mol. Ther.* **3:** 139–148.
7. Reynolds, B. A., and Weiss, S. (1992). Generation of neurons and astrocytes from isolated cells of adult mammalian central nervous system. *Science* **255:** 1707–1710.
8. Ogawa, Y., *et al.* (2002). Transplantation of in vitro-expanded fetal neural progenitor cells results in neurogenesis and functional recovery after spinal cord contusion injury in adult rats. *J. Neurosci. Res.* **69:** 925–933.
9. Lindvall, O., *et al.* (1990). Grafts of fetal dopamine neurons survive and improve motor function in Parkinson's disease. *Science* **247:** 574–577.
10. Freed, C. R., *et al.* (1992). Survival of implanted fetal dopamine cells and neurologic improvement 12 to 46 months after transplantation for Parkinson's disease. *N. Engl. J. Med.* **327:** 1549–1555.
11. Gwynn, B., Lueders, K., Sands, M., and Birkenmeier, E. H. (1998). Intracisternal A-particle element transposition into the murine β-glucuronidase gene correlates with loss of enzyme activity: a new model for β-glucuronidase deficiency in the C3H mouse. *Mol. Cell. Biol.* **18:** 6474–6481.
12. Lois, C., and Alvarez-Buylla, A. (1994). Long-distance neuronal migration in the adult mammalian brain. *Science* **264:** 1145–1148.
13. Ourednik, V., *et al.* (2001). Segregation of human neural stem cells in the developing primate forebrain. *Science* **293:** 1820–1824.
14. Meng, X. L., Shen, J. S., Ohashi, T., Maeda, H., Kim, S. U., and Eto, Y. (2003). Brain transplantation of genetically engineered human neural stem cells globally corrects brain lesions in the mucopolysaccharidosis type VII mouse. *J. Neurosci. Res.* **74:** 266–277.
15. Tamaki, S., *et al.* (2002). Engraftment of sorted/expanded human central nervous system stem cells from fetal brain. *J. Neurosci. Res.* **69:** 976–986.
16. Sferra, T. J., Backstorm, K., Wang, C., Rennard, R., Miller, M., and Hu, Y. (2004). Widespread correction of lysosomal storage following intrahepatic injection of a recombinant adeno-associated virus in the adult MPS VII mouse. *Mol. Ther.* **10:** 478–491.
17. Kopen, G. C., Prockop, D. J., and Phinney, D. G. (1999). Marrow stromal cells migrate throughout forebrain and cerebellum, and they differentiate into astrocytes after injection into neonatal mouse brains. *Proc. Natl. Acad. Sci. USA* **96:** 10711–10716.
18. Sands, M. S., Erway, L. C., Vogler, C., Sly, W. S., and Birkenmeier, E. H. (1995). Syngeneic bone marrow transplantation reduces the hearing loss associated with murine mucopolysaccharidosis type VII. *Blood* **86:** 2033–2040.
19. Dulawa, S. C., Grandy, D. K., Low, M. J., Paulus, M. P., and Geyer, M. A. (1999). Dopamine D4 receptor-knock-out mice exhibit reduced exploration of novel stimuli. *J. Neurosci.* **19:** 9550–9556.
20. Soderling, S. H., *et al.* (2003). Loss of Wave-1 causes sensorimotor retardation and reduced learning and memory in mice. *Proc. Natl. Acad. Sci. USA* **100:** 1723–1728.
21. Rompon, C., *et al.* (2000). Enrichment induces structural changes and recovery from nonspatial memory deficits in CA1 NMDAR-knockout mice. *Nat. Neurosci.* **3:** 238–244.
22. O'Connor, L. H., *et al.* (1998). Enzyme replacement therapy for murine mucopolysaccharidosis type VII leads to improvements in behavior and auditory function. *J. Clin. Invest.* **101:** 1394–1400.

23. Brooks, A. I., *et al.* (2002). Functional correction of established central nervous system deficits in an animal model of lysosomal storage disease with feline immunodeficiency virus-based vectors. *Proc. Natl. Acad. Sci. USA* **99:** 6216–6221.
24. Hayakawa, M., *et al.* (2002). Muscle-specific exonic splicing silencer for exon exclusion in human ATP synthase gamma-subunit pre-mRNA. *J. Biol. Chem.* **277:** 6974–6984.
25. Ichida, M., *et al.* (2000). Differential regulation of exonic regulatory elements for muscle-specific alternative splicing during myogenesis and cardiogenesis. *J. Biol. Chem.* **275:** 15992–16001.
26. Wolfe, J. H., and Sands, M. S. (1996). Murine mucopolysaccharidosis type VII: a model system for somatic gene therapy of the central nervous system. In *Gene Transfer into Neurons: Towards Gene Therapy of Neurological Disorders* (P. Lowenstein and L. Enquist, Eds.), Wiley, Essex.
27. Den Tandt, W. R., and Scharpe, S. (1991). Characteristics of hexosaminidase A in homogenates of white blood cells using methylumbelliferyl-*N*-acetyl-β-D-glucosaminide-6-sulphate as substrate. *Clin. Chim. Acta* **199:** 231–236.
28. Willott, J. F., Turner, J. G., Carlson, S., Ding, D., Bross, L. S., and Falls, W. A. (1998). The BALB/c mouse as an animal model for progressive sensorineural hearing loss. *Hear. Res.* **115:** 162–174.

JOURNAL OF CELLULAR PHYSIOLOGY 208:188–194 (2006)

# Increased Mobilization of c-kit$^+$ Sca-1$^+$ Lin$^-$ (KSL) Cells and Colony-Forming Units in Spleen (CFU-S) Following De Novo Formation of a Stem Cell Niche Depends on Dynamic, But Not Stable, Membranous Ossification

KAZUNARI NAGAYOSHI,[1,2] HIROYUKI OHKAWA,[2] KEIGO YOROZU,[2] MASATO HIGUCHI,[2] SAYUMI HIGASHI,[2] NAOKI KUBOTA,[2] HIROYASU FUKUI,[2] NOBUO IMAI,[2] SATOSHI GOJO,[3] JUN-ICHI HATA,[1] YOSHIRO KOBAYASHI,[4] AND AKIHIRO UMEZAWA[1]*

[1]*Department of Reproductive Biology and Pathology, National Research Institute for Child Health and Development, Tokyo, Japan*

[2]*Chugai Pharmaceutical Co., LTD, Fuji Gotemba Research Institute, Gotemba, Shizuoka, Japan*

[3]*Department of Cardiovascular Surgery, Saitama Medical Center, Kawagoe, Japan*

[4]*Department of Biomolecular Science, Faculty of Science, Toho University, Chiba, Japan*

Stem cells are thought to inhabit in a unique microenvironment, known as "niche," in which they undergo asymmetric cell divisions that results in reproducing both stem cells and progenies to maintain various tissues throughout life. The cells of osteoblastic lineage have been identified as a key participant in regulating the number of hematopoietic stem cells (HSCs). HSCs receive their regulatory messages from the microenvironment in the bone marrow. This would account for a reason why the localization of hematopoiesis is usually restricted in the bone marrow. To clarify the above possibility we employed a cell implantation-based strategy with a unique osteoblast cell line (KUSA-A1) derived from a C3H/He mouse. The implantation of KUSA-A 1 cells resulted in the generation of ectopic bones in the subcutaneous tissues of the athymic BALB/c nu/nu mice. Subsequently the mice obtained a greater amount of the bone marrow than normal mice, and they showed an increased number of HSCs. These results indicate that the newly generated osteoblasts-derived ectopic bones are responsible for the increase in the number of the HSC population. Furthermore, the increased number of HSCs directly correlates with both the magnitude of dynamic osteogenic process and the size of the newly generated bone or "niche." J. Cell. Physiol. 208: 188–194, 2006. © 2006 Wiley-Liss, Inc.

Stem cell with potential for self-renewal and multilineage differentiation can be identified in various self-renewing tissues, including epidermis, intestinal epithelium, and testis, and hematopoietic stem cells (HSCs) are also capable of both self-renewal and multipotency (Ikehara, 2000; Weissman, 2000). The most important experimental evidence for the existence of such cells is the ability of a single bone-marrow-derived cell to reconstitute long-term hematopoiesis in lethally irradiated recipients (Till and McCulloch, 1961; Siminovitch et al., 1963; Till et al., 1964; Matsuzaki et al., 2004). Molecular markers that characterize transplantable cells with stem cell potential and allow their selective purification have been identified, and this achievement has been important to progress both applied and basic science (Spangrude et al., 1988; Goodell et al., 1996). As an example, CD34$^-$, c-kit$^+$, Sca-1$^+$, and Lin$^-$ cells have been identified as the most primitive HSCs (Osawa et al., 1996).

Stem-cell fate decisions in the developing embryo are governed by complex interplays between cell-autonomous signals and stimuli from the surrounding tissues. Stem cells are thought to inhabit in a unique microenvironment, known as "niche," in which they undergo asymmetric divisions that generate both stem cells and progenies to maintain the tissue throughout life (Dzierzak et al., 1998; Matsuzaki et al., 2004). HSCs migrate from the yolk sac to the liver during early development, and they ultimately settle in the bone marrow and spleen of the adult. The bone marrow and spleen serve as the microenvironment that supports the HSCs via cytokines, membrane-bound molecules, and gap junctions. And the classical experiment on HSC-colony formation by Till and McCulloch (1961) showed that reconstitution of hematopoiesis takes place only in hematopoietic organs. The niche hypothesis was first proposed by Schöfield, 1978, and it is supported by the evidence that HSCs have been successfully maintained in co-culture systems with marrow-derived stromal cells in vitro. Steel mice (Sl/Sld) have a mutation at the Sl locus, and spleen colonies cannot be produced in the mice when transplanted with normal marrow cells.



This article includes Supplementary Material available from the authors upon request or via the Internet at http://www.interscience.wiley.com/jpages/0021-9541/suppmat.

Contract grant sponsor: Ministry of Education, Culture, Sports, Science, and Technology (MEXT) of Japan; Contract grant numbers: 14081208, 13470053, 14657051); Contract grant sponsor: Health and Labour Sciences Research Grants; Contract grant numbers: H-14-trans-003, KH71064; Contract grant sponsor: Pharmaceuticals and Medical Devices Agency; Contract grant number: 02-2.

*Correspondence to: Akihiro Umezawa, Department of Reproductive Biology and Pathology, National Research Institute for Child Health and Development, 2-10-1 Okura, Setagaya-ku, Tokyo 157-8535, Japan. E-mail: umezawa@1985.jukuin.keio.ac.jp

Received 26 July 2005; Accepted 13 February 2006

DOI: 10.1002/jcp.20652